8-2020

Genetic Analysis of PI3k and mTOR Inhibition in U87mg Glioblastoma Cell Line

Carl G. Litif
The University of Texas Rio Grande Valley

GENETIC ANALYSIS OF PI3K AND MTOR INHIBITION IN U87MG GLIOBLASTOMA CELL LINE

A Thesis

by

CARL G. LITIF

Submitted to the Graduate College of
The University of Texas Rio Grande Valley
In partial fulfillment of the requirements for the degree of

MASTER OF SCIENCE

August 2020

Major Subject: Biology

GENETIC ANALYSIS OF PI3K AND MTOR INHIBITION

IN U87MG GLIOBLASTOMA CELL LINE

A Thesis
by
CARL LITIF

COMMITTEE MEMBERS

Dr. Megan Keniry
Chair of Committee

Dr. Robert Dearth
Committee Member

Dr. Kristen Lowe
Committee Member

August 2020

ABSTRACT

Litif, Carl, Genetic Analysis of PI3K and mTOR Inhibition in U87MG Glioblastoma Cell Line. Master of Science (MS), August 2020, 42 pp., 2 tables, 9 figures, 23 references

NVP-BEZ235 is a Glioblastoma Multiform chemotherapeutic dual PI3K/mTOR pathway inhibitor created in 2008 and has since been proven experimentally to induce pluripotency in oncological cell populations. The inhibition of PI3K and mTOR has shown to coerce phenotypes associated with stem cell markers, most notably OCT4. It is necessary to understand the genetic composure of how PI3K/mTOR inhibited tumor cells are bypassing the canonical pathway for proliferation and growth and utilizing other parallel sources for tumor invasion into other neural regions. Taking a genetic approach with RNA-sequencing allowed us to gain insight into how glioblastoma interact with cytoskeleton factors MAPK4 and GAP43 to bring up novel phenotypes allowing tumors cells to not only grow but also signal other cells to pick-up a stem-like signature.

DEDICATION

The successful span and finale of my graduate degree in biology are owed in depth to Dr. Megan Keniry who worked with me on end to bring the resilience and intelligence within me out into fruition. I also want to thank my fiancé Andrea Yeoman and my family for being my underlying support throughout all of the strife and thriving moments.

ACKNOWLEDGMENTS

A great deal of gratitude goes towards Dr. Megan Keniry and the graduate lab members Shreya Udawant, Leetoria Hinojosa, David Garza, and Yajaira Macias. Extensive research at all oddball hours was enough to drive one over the edge, yet when you have such a great team who all play a part in something larger than all of us, the amiable mutuality becomes something indispensable to completing a successful graduate thesis and degree.

Support from many professors, faculty, coworkers, and colleagues at UTRGV have changed my outlook on the natural world altogether. I'd also like to acknowledge the opportunities to work with students as a teaching assistant which allowed myself to further grow passion for molecular biology.

TABLE OF CONTENTS

LIST OF TABLES

LIST OF FIGURES

Page

CHAPTER I

LITERATURE REVIEW

Introduction

Glioblastoma multiform (GBM) is one of the toughest cancer types to diagnose and improve prognostically. The shortened life-expectancy that the disease brings upon a person with GBM does not allow *in vivo* studies to be as efficient as other types of cancers out there that the body can essentially endure longer. *In vitro* investigation is caveated with the variability in genetic mutations that create numerous subcategorized phenotypes under the umbrella of GBM which ultimately leads to more questions than answers about which mutated genes are actually coercing such a complex disease. However, a common similarity in these typified brain tumors is the underlying stem-like niche that is allowing tumorigenic cells to proliferate and coerce the invasion of non-affected regions through non-canonical signaling to other cells in proxy.

The phosphatidylinositol 3 kinase (PI3K), mTOR, and Akt pathways are heavily regulated to carry out the growth of a cell. Subtypes of GBM include mutations in these pathways that leave their inhibitory feedback mechanisms diminished or contrarily completely activated. Various chemotherapeutic approaches that target hotspots in these pathways are utilized with limited success due to other regulatory genes that may not be as easily detected during previous. Our approach in this investigation is to utilize genetic approaches such as sequencing the RNA or amplifying genes via polymerase chain reaction (PCR) to gain insight into the dynamic nature that differentiates the chemotherapeutic treated samples from the untreated tumorigenic cell populations.

Glioblastoma Multiforme

Glioblastoma multiforme (GBM) is a high occurring brain tumor that comprises around 25% of total brain tumors, however, GBM is still very rare considering the large amount of known and novel cancers that are out there. Taking these parameters into account with addition to the poor onset of diagnoseable symptoms that lead to low and short survival rates, it has been tough to approach GBM clinically and therefore experimentally (Brennan et al., 2009). Temozolomide is a common alkylating chemotherapeutic that is used simultaneously with radiation treatments for a first line of defense in hopefully what will result in the reduction of slower tumor growth rates thus a decrease in the overall size of a tumor (Brennan et al., 2009). Radiation has been used solely as a treatment for GBM up until 2005 when researchers showed that the treatment in combination with temozolomide chemotherapy showed approximately 3.9-fold increase in rates regarding 5 year-long survivability (Johnson and O'Neill, 2012). Phase III temozolomide clinical testing did not include those that had not undergone bulk-removal of the tumor as well as those aged over 70 years. The testing procedure was also bias towards those that were able to access clinics in which does not truly represent an integrative population of GBM. This led to physicians giving improper diagnoses of 12 months without the chemotherapy and 15 months with both treatments in which many cases did not reach up to those lengths (Johnson and O'Neill, 2012).

Researchers have since brought together data from other sources that are inclusive of the totality of GMB patients with an exclusion to those who had already deceased without having prior lifestyle and tumor treatment information. Johnson and O'Neill analyzed survival rates of 14,000 patients from time periods on either side of the introduction of temozolomide implementation in the summer of 2005. The database was not inclusive of a variable that spoke

as to if the patients had received chemotherapy, but radiation therapy was included in the assessments which served as another limiting factor for choosing which patients to include in the study. Observations showed that the survival rate in total was 8 months with radiotherapy solely and 9 months when both treatments are utilized; 4-5 months lower than that off those patients who had received a form of tumor bulk-removal surgery prior as well. Without any treatment, patients showed survival rate medians of around 3 months (Johnson and O'Neill, 2012).

GBM is commonly classified as being either primary or secondary based upon the severity of presence and prominence essentially. Common pathways leading to GMB tumor phenotypes include mutations to *EGFR, p53, PTEN* and their associated regulatory factors. Further typifying has been carried out regarding the dynamic nature of transcriptomes and their translational outputs followed by essential alterations in post-translational modifications to protein structure. This immensely incorporated regulatory process of gene expression has added to the poor prognosis of when approaching this type of cancer, but researchers have narrowed down most mutations causing tumorigenesis to arise from many tyrosine kinase receptors signaling systems that rely heavily on protein feedback mechanisms. Pathways regulating internal and external signaling such as *SHH, RAS, AKT,* and *WNT* have been shown to have associated factors present at dynamic levels in comparison to their canonical pathway. The gene expression of components within these pathways have been analyzed through genomic, transcriptomic, and proteomic approaches that otherwise have shown correlations of specific mutations throughout various phases within the central dogma (Brennan et al., 2009).

Researchers have shown that GBM tumors can be further classified genetically into three clusters; that of which includes an EGFR core, a PDGF core, or a NF1 core. Extensive analysis of mutations within pathways and overlapping factors that define the aforementioned cores have

been carried out. The EGFR core is comprised of mutations that occur within Notch signaling activity as well as *WNT* subcategories. The EGFR core also includes other ubiquitous signaling factors such as *EIF4EBP1*, *EIF4E*, *RHEB*, and *FGF2*. The PDGF core is defined by upregulations in *PTEN* and *RAS* pathways as well as factors associated with *MTOR* and *FOXO1* regulation. NF1 core has been noted to contain high levels of *IGFBP5* and low levels of NF1. Specifically, the NF1 core also shows decreased levels of *PI3K* and *MAPK* (Brennan et al., 2009).

Phosphatidylinositol 3 Kinase (PI3K) Pathway

The phosphatidylinositol-3 kinase (*PI3K*) pathway regulates cell homeostatic maintenance as well as facilitating the procession of cell cycling. Found in many eukaryotic lineages, *PI3K* is known canonically to phosphorylate phosphatidylinositol 4,5-bisphosphate (*PIP2*) creating phosphatidylinositol 3,4,5-trisphosphate (*PIP3*). *PIP3* will associate with the serine threonine kinase *AKT* which has many identified downstream substrates. Specifically, the *PIK3CA* isoform has been shown as a mutation leading to overexpression in which is causative to tumorigenesis (Martinez et al., 2020).

One of the most common deleterious mutations amongst conventional glioblastoma molecular function is that of the phosphatase and tensin homolog deleted chromosome ten tumor suppressor, or *PTEN*. Associated with phosphatase functions that can degrade and eliminate enzymatic phosphates and enzymes regarding lipid metabolism, *PTEN* is known canonically for the conversion of surface localized phosphatidylinositol (3, 4, 5) triphosphate (*PIP3*) into phosphatidylinositol (4, 5) biphosphate (*PIP2*) by removal of a phosphate group. This conversion carried out by *PTEN* reverses the forward notion of *PIP2* to *PIP3* that is carried out by phosphatidylinositol-3 kinase (*PI3K*) that would otherwise coerce the downstream activity of

PIP3 upon *AKT* which alone leads to an activation of a large repertoire of multifaceted signaling cascades regulating cellular growth and survival physiologies. With *PTEN* in low presence, as seen in many brain tumor types, *PIP3* can no longer be properly regulated by *PTEN* phosphatase activity which in turn will lead to higher cumulative levels of *PIP3* thus facilitating a faltered feedback mechanism that is essentially replicating the presence of external growth factor, insulin, or *RAS* signaling ligands (Keniry and Parsons, 2008).

PIK3CA is a common isoform that drives the canonical production of phosphatidylinositol-3 kinase (*PI3K*) while the highly conserved *PTEN*, downstream of insulin-signaled *PI3K*, is known to eliminate the function of *PI3K*-produced phosphoinositide lipids. *PI3KCA* is common to be constitutively active with low *PTEN* presence in many glioblastoma molecular subsets which has made it a prominent candidate for chemotherapeutic treatment. However, disruptions of insulin regulation occur elsewhere in the body once the pathway itself has become inhibited globally leading to inadequate signaling of insulin in hepatic skeletal-muscular regions and thus bringing upon the onset of hyperglycemia. The insulin homeostatic feedback function to lower blood-sugar concentration kicks back which otherwise reactivates the *PI3K* pathway. This finding depletes the purpose of initial chemotherapeutic agents targeting the *PI3KCA* signaling pathway, especially in those that are insulin resistant due to the increase in hyperglycemic index (Hopkins et al. 2018).

Chemical dousing in combination with radiation, and/or surgical tumor removal has been the common combination therapy prescribed for reducing the presence of GBM. Initial clinical approaches to glioblastoma multiforme (GBM) treatment included simplistic apoptotic-inducing chemotherapeutic agents that invoke DNA damage to set off the alarm for programmed cellular death. The phosphatidylinositol-3 kinase (*PI3K*) pathway as well as the *mTOR* and *RAS*

pathways have been key candidates for inhibitory drug treatments that were thought to reduce cellular survival of the tumor population followed by the predominate enhancing of apoptosis. Inhibiting key components in these signaling pathways singularly shows less effect as when treated with combinatory circumstances giving insight into the non-linear characteristics of cellular proliferation pathways. The efficacy is low for successfully treating patients with chemotherapeutics that are designed with linear approaches to these signaling pathways (Westoff et al. 2014).

Molecular evolution is similar to that of macro-evolution concepts in the likes that inherent explicit complexity being comprised of internal and external factors is linked to the multifaceted approach to carry out a singular purpose of survival. It would be as if looking into a kaleidoscope with a known set of proteins on the end and observing the many formations that are possible. Going further, the various formations of shapes represent diverse interactions amongst conservative pathways that bring upon new protein structures and novel phenotypes. Shifts in cellular environment such as stress stimuli or other signaling factors in excess or depletion lead to the alterations within the internal cellular physiology that are normally handled by specific homeostatic proteins. Alterations, be it anthropogenic or natural, within these pathways leads to novel chemo-sensitive interactions that have been shown to carry out either the same function in redundancy or coerce an unconventional physiology. Specifically, targeting the inhibition of major signaling pathways can lead to high contradiction when novel bypasses are formed, thus meddling with feedback loops that are tightly linked with appropriate cellular function. This type of thinking hypothetically suggests that drug resistance, which is common amongst clinical trials of signaling cascade inhibition in contrast to their initial in vitro success, is linked with novel pathway creation when exposed to inhibitors that has essentially caused a common stream of

many major pathways in which various cancer cell types can then exploit further. This leads to the notion of cell stemness being derived from *PI3K* inhibition and other major proliferative signaling cascades in that other ubiquitous proliferative pathways are now being exploited to essentially redirect traffic after treatment which was designed to block their ultimate function (Westoff et al. 2014).

Mammalian Target of Rapamycin (mTOR) Pathway

mTOR is a serine/threonine protein kinase comprised of 289kDa in which can be canonically found within the *mTORC1* and *mTORC2* complexes regulating growth factor, stress, hypoxic, energetic, and amino acid concentration signaling responses. The *mTORC1* complex is structurally formed by the aggregation of *mTOR* with regulatory-associated protein of mTOR (*RAPTOR*), mammalian lethal with Sec-13 protein 8 (*mLST8*), proline-rich *AKT* substrate 40 kD (*PRAS40*), and DEP domain TOR-binding protein (*DEPTOR*). The complex itself can be inhibited experimentally by rapamycin which targets the 12 kD intracellular FK506-binding protein (*FKBP12*) to facilitate only activity with *mTORC1* leaving *mTORC2* inactive. The pathway in which *mTORC1* is located is downstream of the phosphatidylinositol-3 kinase (*PI3K*) that is the direct facilitator of *AKT* activation by phosphorylation through the preliminary phosphorylation of *PIP2* to *PIP3* which can be reversed by *PTEN*. This pathway in glioblastoma multiform is known ubiquitously to have an altered multifaceted regulation that leads to the onset of tumor phenotypes. Activation of the kinase properties in *mTORC1* canonically occurs via GTPase interaction with the RAS homolog enriched in brain (*RHEB*) that takes place on the tuberous sclerosis complex ½ (*TSC1/2*). From the point at which *mTORC1* is activated via GTP, association with the translational *eiF4E* and ribozymal kinase *S6K* takes place to regulate protein, lipid, and nucleotide synthesis (Mecca et al. 2018).

S6K is able to interact with the 40S ribosomal unit to allow phosphorylation of the substrate which in turn leads to translation initiation of a 5'-terminal oligopolypyrimidine mRNA transcript while also phosphorylating another translation initiation factor, *eIF4B.* The initiation facilitated by *eIF4B* allows aggregation with *eIF3* and *eIF4F,* but it should be noted that the phosphorylation of *4EBP1* via kinase activity within *mTORC1* will lead to *eIF4E's* release from *4EBP1*. This release will free up *eIF4E* allowing the formation of *eIf4E* and *eIF4G*. The *mTORC1* complex also plays a role in activating transcription intermediary factor 1-alpha (*TIF-1A*) which directly will promote RNA polymerase association with rRNA gene loci. *TIF-1A* also inhibits the repressor, *MAF1*, that is associated with RNA polymerase III function. With the promotion of RNA polymerase I and repression of RNA polymerase III, 5sRNA and tRNA transcription can take place effortlessly. Growth factor receptor-bound protein 10 (*GRB10*) is downstream target of *mTORC1* which takes on regulating the denaturation of insulin receptor substrate-1 while also downregulating *PI3K* feedback inhibition (Mecca et al. 2018). Lipid synthesis genes such as *LIPIN-1* lie downstream of the *mTORC1* signaling pathway to downregulate the production of sterol regulatory element-binding protein1/2 (*SREBP1/2*) via constitutive cytoplasmic localization of *LIPIN-1* which otherwise would promote *SREBP1/2* function. Purine production is a downstream target of *mTORC1* activity via the promotion of activating transcription factor 4 (*ATF4*) which further will promote the function of methylenetetrahydrofolate dehydrogenase 2, methenyltetrahydrofolate cyclohydrolase (*MTHFD2*) to regulate the tetrahydrofolate cycle within mitochondria (Mecca et al. 2018).

The complex *mTORC2* which also includes a *mTOR* kinase is uniquely conjoined with rapamycin-insensitive companion of *mTOR* (*RICTOR*), stress-activated map kinase-interacting protein 1 (*mSIN1*), and protein observed with *RICTOR* (*PROTOR*) but also shares structural

components included in the *mTORC1* complex. *DEPTOR* and *mLST8* are found in the *mTORC2* complex but in this setting, they help facilitate the insensitivity to rapamycin in that *FKBP12* cannot be associated with *mTORC2* complex unlike *mTORC1* which is inhibitable by rapamycin. Activation of the *mTORC2* complex is facilitated by the response of growth factors but not nutrient stimulation. Downstream of *mTORC2*, essential processes regulating cell motility, proliferation, and survival through a diverse set of *AGC* protein kinases. Key members of the *mTORC2* stimulated *AGC* protein kinases are various isoforms of protein kinase C (*PKC*) that are known for involvement in cytoskeleton dynamics to coerce cell migratory efforts (Mecca et al. 2018).

Common mutations that define glioblastoma multiform include the inhibition of *PTEN* and constitutive activation of *PI3K* that result in a mimicry of *EGFR* signaling characterizing these tumor types as *EGFR*-independent. One of the targets of *PI3K* activity is the production of *PIP3* from *PIP2* which is a trigger for indirectly promoting the *mTOR* kinase responsible for a plethora of cell metabolic processes. *mTORC1* phosphorylates threonine 389 on *S6K1*, serine-209 on *eIF4E* while the *mTORC2* complex phosphorylates serine-473 on *AKT* and glucocorticoid-induced protein kinase (*SGK*). *mTOR* has a similar domain like that of *PI3K* which is how dual inhibition via NVP-BEZ235 is possible. Inhibition of the *mTORC1* complex via downregulation of *S6K1* activity leads to a negative feedback loop caused by *IRS-1* that will increase phosphorylated *AKT*. On the contrary to allosteric inhibitors, ATP-competitive inhibitors decrease the phosphorylation of *AKT*, and it is still unsure why (Fan and Weiss, 2012).

NVP-BEZ235: PI3K & mTOR Dual Inhibitor

The *mTORC1* complex has been shown to decrease the feedback inhibition system that regulates *PI3K* activity leading clinical investigators to believe that dual inhibition of *PI3K* and

mTOR would results in a decrease of the proliferative pathway in general. Dual inhibitors of *PI3K* and *mTOR* are classified as ATP-competitive meaning they directly target the kinase domains of each protein kinase. Inhibition leads to G1-G0 cell cycle arrest that essentially slows the growth of the tumor. NVP-BEZ235 in 2016 was in phase I testing clinically and is now in phase II showing promising bulk removal of tumors. However, it is important to consider the novel and minute heterogenous features that define glioblastoma multiform. Bypassing systems of inhibitory intervention is a common drug-resistant method that tumor populations undergo which can lead to increased complexity in a series of non-canonical pathways. NVP-BEZ235 is, however, much better at gaining adequate pharmacokinetic measures for treatment purposes (Li et al. 2016).

Glioblastoma & Stem Signature

Glioblastoma has been shown to have persistent stem-like populations even after various chemical treatments have targeted multiple points in pathways regulating cellular proliferation, adherence, and pluripotency (Wang and Herlyn, 2015; Li et al., 2016). There are specific markers for stemness that are canonically seen in tissues with stem cells which have nuanced roles when up or down regulated in tumor environments. Octamer binding transcription factor 4 (*OCT4*) with its isoforms, SRY-box containing protein (*SOX2*), *NANOG* and various alkaline phosphatases are considered signatures that are irregulated in adult aromatic cells that have stem-like phenotypes leading to proliferation of mutated tumor cells that otherwise would follow apoptotic routes (Zhang et al., 2014; Poursani et al., 2016). *OCT4* is a known transcription factor that is phosphorylated by *AKT*, a downstream target of the *PI3K* pathway, to promote a feedback loop that promotes *AKT1* to facilitate activation of pathways downstream of *PI3K* even when inhibited. These two pathways – *OCT4* and *AKT* – when inhibited or knocked down have shown

to slow tumor spread by not allowing the factors and other stem transcription factors or post-transcriptional modifiers to become associated with DNA directly and in appropriate position to coerce the activation of chromatin remodeling genes (Li et al., 2016; Zhao et al., 2014; Zhang et al., 2014).

OCT4B1 specifically has been shown to coerce anti-apoptotic factors and block environmental toxic signaling when located within the nucleus and cytoplasm unlike *OCT4A* isoforms which are seen primarily within the nucleus solely. Knockdown of *OCT4B* has also been shown to decrease cellular proliferation while ectopic expression led cellular colonies to grow at faster rates. Looking into genome databases has shown that prognosis correlation amongst patients who express high-levels of *OCT4B* is considered significantly different than the patients' prognosis with low-levels of *OCT4B*; *OCT4A* showed no significant difference between those sample groups with high and low *OCT4A* expression (Choi et al., 2019; Poursani et al., 2016).

Interleukin-6 is a cytokine factor known to play a role in associating with the glycoprotein *GP130* to promote activation of downstream *MAPK*, *AKT*, and *mTORC* pathways while also facilitating activation of transmembrane receptor proteins (Jones and Jenkins, 2018). Leukemia inhibitory factor (*LIF*) is another cytokine that activates *PI3K* by associating with the same *GP130* recpetor but in another mechanism different from *IL-6*. Both *IL-6* and *LIF* are known to associate with activation of *MAPK* leading to other phenotypes that coerce proliferation of cells that are tumorigenic (Onishi and Zandstra, 2015; Jones and Jenkins, 2018).

Cytoskeleton Signaling

Brain tumors can be classified by their genotypic alterations into two subgroups: less common oligodendroglioma genotype are noted for mutations within both isocitrate

dehydrogenase isoforms caused by deletions within the 1p and 19q chromosomal regions in which is characteristically atypical within the more common astrocytoma genotype. Astrocytoma brain tumors are classified into 4 categories related to a severity gradient – I, II, III, and specifically the IV type that is known as glioblastoma (Osswald et al. 2015).

Cell to cell contact and further signaling occurs via mediating microtubules extending from the membrane which was first shown in developmental phases within Drosophila. Since the novel finding, proof of organelle transport, stem signaling, and differentiating cell-cell coupling has been shown to occur within what are known now as cytonemes, or membrane nanotubes that are the size of less than 1 um in width. The cellular membrane projections have been shown to also have actin-foci as well as other ubiquitous cytoskeleton elements including myosin II-A, beta-catenin, and beta-parvin, but it should be noted that not all elements – N-cadherin, myosin X, and beta-tubulin III - of the cytoskeleton are in use and even molecular refinement has taken place to strategically utilize only a specific concoction for cytoneme regulation. Arborization was also seen and noted to be correlated with dendritic phenotypes. The cytoneme projections showed presence of mitochondria as well as evidence of vesicular trafficking leading to believe that cell to cell signaling in tumors that otherwise facilitates diffusive growth to other pluripotent cells is regionalized in this area (Osswald et al. 2015).

Extensive confirmation of genotypes for over 250 glioblastoma samples revealed that connexin 43 (*Cx43*) is predominately responsible for mediating the creation of the cytoneme projections. Inhibition of the surface adhesion factor led to a decrease in the overall cytonemic production that led to promising results of decreased tumor size in vivo. *Cx43* was also found not only to induce the cytoneme production for tumor signaling, but also to serve as a radiotherapeutic resistant feature that when inhibited will allow the treatment to further reduce

cytoneme presence Also, the phospholipase C regulatory pathway has been shown to be involved in neurite projections regarding tumor cell proliferation and motility into other areas diffusively (Osswald et al. 2015).

GAP-43 in the likes of *Cx43* was found to be in high quantities both genotypically and actually physically localized to cytoneme regions. Overexpression of *GAP-43* led to increased formation of the projections as well as increased tumor size while contrarily, when knocked down and inhibited, the projections were decreased in presence that correlated with decrease in overall tumor diffusiveness, proliferation, cellular density, and overall size of the glioblastoma. To support the role of *GAP-43* in cytoneme production, the nanotube structures formed in significant amounts when *GAP-43* is overexpressed in oligodendroglioma cell lines that are known the be 1p/19q co-deleted and otherwise do not show cytoneme phenotypes (Osswald et al. 2015).

Mitogen activated protein kinase 4 (*MAPK4*) has been shown to interact with *AKT* and *mTORC2* via direct phosphorylation that leads to both of these pathways becoming activated thus leading the cell to have an enhanced proliferative phenotype. *MAPK4* is thought to allow the bypass of *PI3K* inhibiting drugs to activate downstream *AKT* (Wang et al., 2019).

CHAPTER II

METHODOLOGY

Cell Culture

The glioblastoma multiform cell line *U87MG* was acquired from American Type Culture Collection (ATCC) from Manassas, VA and maintained in standard cell culture growth conditions at 37 degrees Celsius in a Dulbecco's Minimal Modified Eagle Medium (DMEM) consisting of 5% CO2, 10% fetal bovine serum (FBS), and 5% of an antifungal & antibacterial treatment; grown in 10cm dish. Confirmation to ensure the absence of contaminant mycoplasma species was analyzed with MycoAlert Detection Kit. Control group was treated with DMSO vehicle; treatment group was exposed to a clinical 50nM dosage of *PI3K*/*mTOR* dual-inhibitor NVP-BEZ235 which was acquired from Sigma in St. Louis, MO. A series of extractions for RNA isolation occurred at various time increments from 6 hours to 9 days.

RNA Isolation

MiniPrep RNeasy isolation kit was sourced from Qiagen in Hilden, Germany which was used to extract cellular contents while enriching for RNA and decontaminating DNA residues. Control and treatment cell culture plates were both washed twice with 2 mL of PBS buffer followed by a 10 uL to 1 mL ratio of BME and RLT buffers. An RW and ethanol wash at a 1:1 ratio was then given. Spin-columns were used to isolate and enrich for RNA while using RQI DNase buffer and RW buffer to remove DNA contamination. After centrifugation, isolates were analyzed for RNA content via observation of spectrophotometer absorbance. Samples were then kept frozen at 80 degrees Celsius.

cDNA Preparation

Isolates from RNA extraction were transformed via thermocycling into cDNA utilizing Superscript Reverse Transcriptase II sourced from Invitrogen in Carlsbad, CA. cDNA was stored in freezing conditions until ready for use in diluted allocates.

Quantitative Real-Time Polymerase Chain Reaction (qt-PCR)

Gene expression analysis was completed utilizing diluted cDNA, Power SYBR Green Master Mix from Applied Biosystems in Foster, CA, distilled water, and diluted primers. Primers were designed using NCBI genetic database sequence information and inputting specific regions into primer3 (v 0.4.0) to create forward and reverse primer sequences. Primers sequences were then out-sourced to Sigma-Aldrich in St. Louis, MO for lyophilized primers which were diluted in house to 10 uM for PCR analysis in an Illumina Eco Real-Time qt-PCR machine from San Diego, CA. Normalization was taken into account through calculation of $2^{-\Delta\Delta CT}$, where CT stands for cycle threshold, or the cycle our of 40 in which the gene was amplified enough to be considered expressed in vitro. Quantitative data for the normalized CT average of four replicates per gene was then calculated for the log2 fold change resulting in a single variable that represents differential genetic expression between the control and treated sample groups. Graphical representations of qt-PCR data were configured and included in the appendix.

Western Blot

BioRad protocol was used for completing western blot protein analysis. Development of transferred proteins on the polyacrylamide gels onto a nitrocellulose membrane and further exposure in the BioRad ChemiDoc allowed fluorescence of specific antibodies to be observed. Cell isolates were utilized from previous 24 hr. and 9 day *U87MG* cell cultures treated with

various drugs affecting specific pathways within the *PI3K*/*mTOR*/*AKT* pathways. *OCT4* (2840) and *OCT4A* (2750) antibodies were used for detection and confirmation of PCR gene expression.

Regression Analysis

Regression of PCR gene expression results was carried out utilizing SAS statistical programming software. Multiple multivariate situations reflecting correlations between *OCT4* isoforms, stem genes, and signaling factors were examined to construct an idea of the relationship amongst these genetic factors that are known to be present in NVP-BEZ235 samples. The analysis should also reveal insight into the niche behavior of embryonic and somatic stem-cells and help determine the physiological nature of oncogenic cell populations. The 'sample' is a nominal independent dichotomous variable signifying whether the sample is a control (0) or treated with NVP-BEZ235 (1). *OCT4A1/A2/A3/B1/B2, LIF, IL6, SOX2, NANOG*, and *OCT4* (complete) are variables utilizing an interval scale of measurement to represent a relative and quantifiably comparable value of gene expression without a true meaning of zero yet still reflects a quantifiable comparison. The cycle threshold (CT) value of the target gene is used to represent the cycle in the PCR (out of 40) in which a threshold of amplification has been surpassed signifying the gene was amplified and is present significantly. However, there is a necessity to take background fluorescence into consideration which is taken care of by a differential adjustment using an internal reference gene (*GAPDH*).

RNA-Sequencing

RNA from cell cultured plates for both the control and treatment groups were isolated to equal concentrations allowing for the necessary 3 replicates with the threshold of RNA integrity met. Stem gene expression and concentration of RNA had to be optimized numerous times to reflect the differentiation between the treatment and control groups which otherwise were

obvious in lower concentrations. There was a necessity for culturing a larger number of treated cells to equivalate the RNA concentration of control cells that had a higher survival rate and were not at risk to RNA degradation thus in turn having higher RNA concentrations. This led to the necessity to culture 20 plates of the treated group while only culturing 3 plates of the control which again was sufficient in terms of proper RNA concentration and integrity.

Illumina RNA-sequencing was out-sourced to Novogene Co. in the University of California at Davis for differentially expressed gene (DEG) analysis between the two control and treatment groups. Mapping and alignment of FASTA sequence reads to the human genome were completed by Novogene Co. Further analysis of DEG was completed by Novogene taking into consideration false discovery rate in the read counts (Benjamin-Hochberg). Read counts were normalized into FPKM values. Transformation of this data into graphical figures and tables is located in the appendix. Gene ontology analysis from DEG data utilizes a database to reflect the genes in our samples with correlation to specific molecular pathways withing cells. One limitation of RNA-sequencing is the background noise of housekeeping genes that are generally at consistent high levels within the cellular life cycle which can overshadow genes that are still differentiated between control and treatment groups.

Gene Set Enrichment Analysis (GSEA)

Gene set enrichment analysis was carried out using software offered from the Broad Institute server. False discovery is also taken into consideration with regards to the size of the gene set being analyzed for. This analysis examines the DEGs in the samples in terms of specific categorical gene sets that are comprised of similar genes within a pathway, cellular function, or molecular structure.

CHAPTER III

RESULTS

Genetic Expression of OCT4 Isoforms

To explore further into the role that *OCT4* has in facilitating a stem-like phenotype in glioblastoma tumor populations, curated primers of *OCT4* isoforms were designed with the intention to create isolated *OCT4* variant transcripts of *POU5F1* without background noise from pseudogenes. Previous research has shown that OCT4 isoforms – *OCT4A1, OCT4A2, OCT4A3, OCT4B1, OCT4B2* – are correlated with different cellular physiologies depending on tissue type and further have nuanced mutations allowing the onset of various types of cancer. Treating the *U87MG* cells with NVP-BEZ235, an inhibitor for the *PI3K* and *mTOR* pathways, allows investigation into the small population of cells which bypass apoptosis in which the drug would normally induce. Stem-cell marker *OCT4* and other high mobility groups associated with the transcription factor interact directly with *FOXO* homeobox regions to facilitate an unknown mechanism keeping *FOXO* nuclear active thus allowing downstream activation of stem cell homeostatic mechanisms. In glioblastoma tumors, *OCT4* isoforms' association with *PI3K* and *mTOR* pathways is poorly understood regarding the nature of how this stem-like phenotype persists even after major growth pathways have been inhibited chemically. Figure 1A shows significant *OCT4* isoform genetic expression compared to the complete *OCT4* (depicted as *OCT4A*) primer sequence. The log2fold change of the isoforms ranged from 2.9 to 5.2 with *OCT4B1* having the highest expression while *OCT4A1* had the lowest which was very similar to the expression of the complete *OCT4* gene. Figure 1B shows a genetic expression time course

for the complete transcript of *OCT4* which was used to optimize support the days chosen for further investigation into the study; days 3-6 were inclusive of the peak for *OCT4* genetic expression and were thus chosen as a suitable range for further analysis.

Western blot analysis in Figure 1C was completed alongside qt-PCR to confirm the protein presence of the C-terminal portion of *OCT4* (*OCT4A* - 2840 antibody) compared to the complete protein *OCT4* (2750 antibody). Various pathway points of *PI3K/AKT/mTOR* were inhibited utilizing various inhibitory drug treatments – DMSO (control), NVP-BEZ235 (*PI3K*/*mTOR* inhibitor), BKM120 (*PI3K* inhibitor), MK226 (*AKT* inhibitor), Rapamycin (*mTOR* inhibitor), and insulin to promote growth – to give insight into the proteomic expression of *OCT4A* regions versus the complete *OCT4* protein inclusive of *OCT4B* isoforms. Time scale falls on two extremes of 24 hours and 9 days to give allow observe dynamics of *OCT4* over time when treated with NVP-BEZ235. Contrary to the qt-PCR results showing *OCT4A1/A2/A3* isoform presence, fluorescence of the *OCT4A* isoform via antibody (2840) targeting to the C-terminal region was surprisingly was not detected in the *PI3K*/*mTOR* inhibited cell lines compared to the *OCT4* complete antibody (2750). This could be due to post translational modifications that have been shown to affect *OCT4* and therefore lead to an alteration of confirmation which could disrupt the detectability of the *OCT4A* region. Further Analysis of modifications should be considered as well as investigation utilizing *OCT4B* specific antibodies and refined *OCT4A* antibodies.

Loading control of the blot needs further optimization as the fluorescence of *GAPDH* internal controls were not completely equivalent even after a first round of optimization – amounts of loaded material located in the methods section. What can be taken from this protein presence analysis is confirmation of *OCT4* having two prominent bands between the 37 kD and

50 kD marker ladder references. This could be a result of two regions of *OCT4* (*OCT4A* and *OCT4B*) being translated leading to the antibody detecting both products. Further analysis of antibodies utilized for *OCT4* isoform investigation would be noteworthy and insightful into what exactly is being produced as PCR analysis promotes conflicting results with presence of *OCT4A* antibodies.

You can also determine from the blot (Figure 1C) that a decrease in NVP-BEZ235, BK226(PI3K inhibitor), and rapamycin (mTOR inhibitor) treated cell populations from 24 hours to day 9 are similar compared to the increase in population seen in the insulin treated and somewhat in the *AKT* inhibited. This could be due to the nature of the drugs which are inhibiting growth pathways and essentially triggering apoptosis in the cells. Presence of two bands is stronger at 24 hours while only one band is prominently seen in the day 9 lysates leading us to believe that there is one *OCT4* isoform preferred over the other in regulating these stem-like growth phenotypes or another cellular mechanism involved in cell-cell signaling of immune factors. The size of the *OCT4A* protein in which the antibody is targeted for is around 45-47 kD while *OCT4B* in general range from 20-43kD, so this leads us to believe that *OCT4A* is playing a role that the PCR results confirm. In general, this *OCT4* presence in glioblastoma cell line *U87MG* leads us to believe that this type of tumor population has presence of stem-cell niches that coerce a tumorigenic phenotype (Zhao et al., 2014; Wang et al., 2015).

Figure 3A shows the results of a linear regression analysis intended to test for a significant correlation of *OCT4* isoforms and other stem markers between the DMSO control and NVP-BEZ235 treated samples; all transcripts tested showed a significant difference between the sample groups. Analysis of the correlation between onset of *OCT4A* and *OCT4B* isoforms dependently (Figure 3B,3C) showed a high correlation between the two significantly expressed

isoform subgroups. When looking into the correlation between *OCT4* isoforms and the complete *OCT4* transcript inclusive of both C and N domains (Figure 3D), only *OCT4B1* was significantly correlated with the onset of both regions. Similar results in figure 3F associate only the *OCT4B1* isoform significantly with the presence of *LIF* and *IL-6* factors. *OCT4B1* and these factors have all been associated with immune functions in literature and further investigation would prove insightful.

Genetic Expression of Stem Cell Markers

Glioblastoma cell line *U87MG* was treated with NVP-BEZ235, a *PI3K*/*mTOR* dual-inhibitor, and cultured for six days followed by RNA isolation for PCR analysis of stem cell markers SRY-Box transcription factor 2 (*SOX2*), alkaline phosphatase intestinal (*ALPI*), alkaline phosphatase placental (*ALPP*), alkaline phosphatase biomineralization (*ALPL*), alkaline phosphatase germ cell (*ALPG*), and *NANOG* homeobox. Stem signatures in canonical stem-cells are characterized by these specific genes and were chosen for further investigation to support the claim that heightened *OCT4* presence in *PI3K*/*mTOR* inhibited cell lines is what is driving the proliferation of the tumor population after initial chemotherapeutic treatment. Table 1 describes the primer sequences used in these analyses.

Stem markers *SOX2* (a high mobility group correlated with *OCT4*), and *NANOG* were examined for genetic expression between the control and treated samples. Figure 2A depicts the significantly increased presence of *NANOG* having a log2fold change of 6.5 while showing *SOX2* with significant increase around 1.9-fold, however, the error should lead us to question the data and further explore the presence of *SOX2* within these cell populations. Figure 3E shows a significant correlation of *SOX2* and *NANOG* amongst the presence of all *OCT4* isoform

transcripts allowing us to conclude that the increased presence of *OCT4* presence due to PI3K/mTOR inhibition is supported by other stem niche markers.

Figure 2B shows the log2fold changes of *ALP* isoforms between the control and NVP-BEZ235 treated groups. *ALPG* and *ALPI* were notably increased in genetic expression by almost 2.5-fold compared to *ALPL* and *ALPP* which averaged around a 1 to 1.5-fold change. Further regression analysis must be completed to assess the significant correlation.

Genetic Expression of Cell-Cell Stem Signaling Factors

Cell-cell stem signaling components leukemia inhibitory factor (*LIF*) and interleukin 6 (*IL6*) were examined for genetic expression to again support the claim that there are other factors involved in coercing a stem-like phenotype in glioblastoma alongside expression of *OCT4* and other stem markers. Both components increased in log2fold change however, there was a large difference between the control and NVP-BEZ235 treated samples regarding LIF which had an erroneous 4-fold increase compared to *IL-6* that had a 36 log2fold increase (Figure 2C). Multivariate analysis of *OCT4* isoforms and these two cell-cell stems signaling factors displayed in figure 3F show only a significant correlation with the presence of the *OCT4B1* isoform.

RNA-Sequencing: Differentially Expressed Gene Analysis

A genetic approach was taken to quantify the differentially expressed genes (DEG) between the control and NVP-BEZ235 treated samples. Optimization of time points (Figure 1E) and density of initial cell culture (Figure 4) was a crucial limiting factor in the timeline of this approach. After months of various optimization experiments with variations in plate size, RNA column loading protocol, density of cell population, and time point of extraction for RNA isolation led us to use a protocol described in chapter III with 10 cm plates holding 2 mL of media with extraction of RNA occurring on day 3. The results of this density analysis gave

insight into what occurs to the *OCT4* genetic expression as the plate becomes more populated and perhaps diluted within the mass of cells.

RNA was out-sourced to Novogene for RNA sequencing, mapping, aligning, and further analysis of DEG. Out of around 58,000 gene configurations, approximately 8,000 were significant in being expressed differentially between the two sample groups: control and NVP-BEZ235 treated. Figure 5 shows the -log2fold change for some of the highest and lowest genes that were expressed differentially in specific gene ontology (GO) categories which were the expressed the highest as seen in Figure 5 and 6. “Cell adhesion molecule binding” in Figure 6 was of significant molecular interest alongside the highly expressed “cell-substrate adherens junction” cellular component pathway depicted in Figure 7. These GO categories represent over 200 genes involved in cellular surface interactions. To support the claim that there are surface components undergoing dynamic phenotypes in *PI3K*/*mTOR* inhibited cells, Figure 6 shows that “focal adhesion”, “actin cytoskeleton”, “microtubule”, and “collagen-containing extracellular matrix” categories had a high number of genes expressed in similarity to the “cell-substrate adherens junction” leading us to believe that there is a change in surface morphologies that are leading to proliferation of glioblastoma.

Qt-PCR screening was completed with results in Figure 8 for 25 of the genes depicted in Figure 5. *MAPK4* and *GAP43* became of particular interest as they have been shown in previous research to be correlated with the above categories mentioned from Figure 6 and 7. A gene set enrichment analysis (GSEA) and heatmap analysis (Figure 9) were completed to analyze a plethora of pathways that were differentially expressed in regards to specific gene sets, or a groups of genes that relate to one cellular function etc. Out of the many enriched pathways, it was of particular interest to look into the “BIOCARTA MAPK PATHWAY” enrichment

showing the multitude of *MAPK* isoforms involved in many unique cellular functions. *MAPK4* was of the highest to be enriched in NVP-BEZ235 samples supporting the qt-PCR evidence. Further gene sets should be characterized for glioblastoma types which is where data from this RNA-seq should go towards in future studies i.e. *GAP43* and *MAPK4* defining severe levels of glioblastoma that have attained malignant growth phenotypes.

CHAPTER IV

DISCUSSION

Glioblastoma multiform is a one of the most aggressive forms of cancer characterized by low prognosis and survival time once diagnosed adequately which itself is an unsure and time-consuming. Glioblastoma spreads in the brain more like a degenerative disease would in that invasion of neural networks becomes the prime characteristic to coerce the spread of malignancy. Taking data from the PCR, western blot, and RNA-seq analyses led our lab to confirm previous research that proposes stem-like cell signatures within oncogenesis. Looking deeper into *OCT4* isoforms allowed us to conclude that the two subcategories *OCT4A* and *OCTB* are both necessary for genetic expression of either one, however proteomic expression contradicted this evidence with one antibody in that the *OCT4A* regions were not expressed as compared the entire *OCT4* complete transcript antibody. However, the banding patterns of the *OCT4A* complete transcript show that there is still presence of the *OCT4A* isoform at around 46 kD and another isoform at around 37 kD which correlates with previously determined sizes of *OCT4* isoforms.

Translational modifications could be a reason why this is the case. *OCT4B1* was also notably the only significant isoform to correlate with *LIF* and *IL-6* stem signaling molecules as well as the only isoform that significantly was related with the onset of the entire *OCT4* transcript. Further investigation would give insight to whether or not there is a direct association amongst these three factors to promote immunological supported stem-like phenotypes. While *OCT4A* is seen to be present in genetic expression, it could be that *OCT4B1* is regulating the

bypass of PI3K's influence of *AKT* activation with direct interaction with activating *AKT1* via a positive feedback loop.

Optimization for the samples of RNA-sequencing proved to be the limiting factor for a genetic investigative approach. Many variables in drug dose, plate size, cellular density, time points, and alterations in RNA isolation protocol were necessary to experiment with in order to reach the threshold for adequate RNA integrity. Results from the RNA-sequencing were quite interesting in regarding the cellular surface adhesion and cytoskeleton GO pathways that were enriched in the treated samples. *MAPK4* and *GAP43* are of particular interest for further study as previous literature has shown that these expressions represent a glioblastoma subtype which subsists off of bypassing the *PI3K*/*mTOR*/and *AKT* pathway to coerce tumor cell proliferation while staying in a stem-like phenotype. Microtubule projections are associated tightly with *MAPK4* activity while *GAP43* is tightly linked with growth patterns for neural cellular body projections. Together these genes are thought to bypass proliferative regulatory pathways that otherwise are inhibited by chemotherapeutic approaches to coerce invasion into other regions of neural tissue. Future investigation regarding these two genes would shed light onto how glioblastoma spreads quickly into regions of the brain causing fatality.

REFERENCES

Auvergne, R. et al. 2013. Transcriptional distinctions between normal and glioma derived A2B5+ progenitor cells identify a core set of genes dysregulated at all stages of gliomagenesis. *Cell Rep* 3(6): 2127-2141

Brennan, C., et al. 2009. Glioblastoma Subclasses Can Be Defined by Activity among Signal Transduction Pathways and Associated Genomic Alterations. *PLoS ONE* 4(11): e7752

Choi, S. et al. 2019. OCT4B Isoform Promotes Anchorage-Independent Growth in Glioblastoma Cells. *Molecules and Cells* 42(2):135-142

Fan, Q. and Weiss, W. 2012. Inhibition of PI3K-Akt-mTOR signaling in Glioblastoma by mTORC1/2 Inhibitors. *Methods of Molecular Biology* 821:349-359

Hopkins, B. et al. 2018. Suppression of Insulin Feedback Enhances the Efficacy of PI3K inhibitors. *Nature* 560(7719):499-503

Johnson, D. and O'Neill, B. 2012. Glioblastoma survival in the United States before and during the temozolomide era. *Journal of Neuroöncology* 107:359-364

Jones, S. and Jenkins, B. 2018. Recent insights into targeting the IL-6 cytokine family in inflammatory diseases and cancer. *Nature Reviews Immunology* 18: 773-789

Keniry, M. and Parsons, R. 2008. The role of PTEN signaling perturbations in cancer and in targeted therapy. *Oncogene* 27:5477-5485

Kölsch, V., et al. 2007. The Regulation of Cell Motility and Chemotaxis by Phospholipid Signaling. *Journal of Cell Science* 121:551-559

Li, W. et al. 2016. Dual inhibiting OCT4 and AKT potently suppresses the propagation of human cancer cells. *Scientific Reports* 7: 46246

Li, X., et al. 2016. PI3K/Akt/mTOR signaling pathway and targeted therapy for glioblastoma. *Oncotarget* 7(22):33440-33450

Liu, Z., et al. 2011. Activation of ERK1/2 and PI3K/Akt by IGF-1 on GAP-43 Expression in DRG Neurons with Excitotoxicity Induced by Glutamate In Vitro. *Cell Molecular Neurobiology* 32:191-200

Martinez, E., et al. 2020. The PI3K pathway impacts stem gene expression in a set of glioblastoma cell lines. *Journal of Cancer Research and Clinical Oncology* 146:593-604

Mecca, C., et al. 2018. Targeting mTOR in Glioblastoma Rationale and Preclinical/Clinical Evidence. *Disease Markers* 9230479

Onishi, K. and Zandstra, P. 2015. LIF signaling in stem cells and development. *Development* 142: 2230-2236

Osswald, M., et al. 2015. Brain Tumor Cells Interconnect to a Functional and Resistant Network. *Nature* 528:93-98

Osswald, M., et al. 2019. Tunneling nanotube-like structure in brain tumors. *Cancer Reports* 2: e1181

Poursani, E. et al. 2016. Differential Expression of OCT4 Pseudogenes in Pluripotent and Tumor Cell Lines. *Cell Journal* 18(1): 28-36

Wang, W., et al. 2018. MAPK4 overexpression promotes tumor progression via noncanonical activation of AKT/mTOR signaling. *Journal of Clinical Investigation* 129(3):1015-1029

Wang, Y. and Herlyn, M. 2015. The emerging roles of OCT4 in tumor-initiating cells. *American Journal of Physiology – Cell Physiology* 309: C709-C718

Westhoff, M., et al. 2014. A critical evaluation of PI3K inhibition in Glioblastoma and Neuroblastoma therapy. *Molecular and Cellular Therapies* 2:32

Zhang, X. et al. 2014. FOXO1 is an essential regulator of pluripotency in human embryonic stem cells. *Nature Cell Biology* 13(9): 1902-1099

Zhao, Q. et al. 2014. Akt-mediated phosphorylation of Oct4 is associated with the proliferation of stem-like cancer cells. *Oncology Reports* 33: 1621-1629

APPENDIX

TABLES AND FIGURES

#	GENE	DESC	F/R	PRIMER SEQ	#	GENE	DESC	F/R	PRIMER SEQ	#	GENE	DESC	F/R	PRIMER SEQ
1	**FAP**	fibroblast activation protein alpha	**F**	ATTTGGAGTTGCCACCTCTG	15	**WNT9A**	wingless-type MMTV integration site family member 9A	**F**	CTCGAGTGCCAGTTCCAGTT	30	**OCT4A2-1**	OCT4A2 Isoform - First Round	**F**	TAAGCTTCCAAGGCCCTCCT
			R	AAAATATCCTTCAGTGTGAGTGC				**R**	CGAGGAGATGGCATAGAGGA				**R**	GCCCACAGTACGCCATCC
2	**FGR**	FGR proto-oncogene Src family tyrosine kinase	**F**	CAACCCTGGCTTCCTTGATA	16	**MAP7D2**	MAP7 domain containing 2	**F**	CAGGGAAGATCGCAGAACC	31	**OCT4A1-2**	OCT4A1 Isoform - Second Round	**F**	TGAGTAGTCCCTTCGCAAGC
			R	CCCTTGGTGAAGGTGAGGT				**R**	TCTTTCTTCTCGTCTTTCTTTGG				**R**	CTTGGCAAATTGCTCGAGTT
3	**FGF17**	fibroblast growth factor 17	**F**	AGCTGCTGATTCTCTGCTGTC	17	**IGFBP3**	insulin like growth factor binding protein 3	**F**	GTCAACGCTAGTGCCGTCAG	32	**OCT4A2-2**	OCT4A2 Isoform - Second Round	**F**	GGGGTTGAGTAGTCCCTTCG
			R	ACGTGCTTGCCACTGGTC	133-1026			**R**	GACGGGCTCTCCACACTG				**R**	TGCAGAGCTTTGATGTCCTG
4	**GPR3**	G protein-coupled receptor 3	**F**	GAGCGGTACCATGATGTGG	18	**INHBE**	inhibin beta E	**F**	ACTACAGCCAGGGAGTGTGG	33	**OCT4A3-2**	OCT4A3 Isoform - Second Round	**F**	GTGGAGAGCAACTCCGATG
			R	CTTAGGCGAGGGCAGTGGT				**R**	GACCGAGGAGTGGACAGGT				**R**	TGCAGAGCTTTGATGTCCTG
5	**FHAD1**	forkhead-associated (FHA) phosphopeptide binding domain 1	**F**	AAATAAAAGTACCACAATTGGAAGG	19	**TMEM255A**	transmembrane protein 255A	**F**	CATCAGTCCCTGACTCAGCA	34	**OCT4B1-2**	OCT4B1 Isoform - Second Round	**F**	GCTCCTGAAGCAGAAGAGGA
			R	TGGAGAACAAAGCTGCACTC				**R**	CAAGGCCCACTGTGAGAATTA				**R**	AGCTAAGCTGCAGAGCCTCA
6	**SHANK1**	SH3 and multiple ankyrin repeat domains 1	**F**	CAGCATGATGGTCTTCAGGA	20	**ERRFI1**	ERBB receptor feedback inhibitor 1	**F**	CCATGGGGAATATGAGGAAG	35	**OCT4B2-2**	OCT4B2 Isoform - Second Round	**F**	AGTGATTCTCCTGCCTCAGC
			R	CTCTCGCTCAGGGCACAG				**R**	ATTAGGCGCTCCTGAGCAGA				**R**	ATCCCAGGGTGATCCTCTTC
7	**GAS6**	growth arrest specific 6	**F**	TACCCAAGATACTTAGACTGCATCA	21	**NRG1**	neuregulin 1	**F**	TGGGAATGAATTGAATCGAAA	36	**ALPI**	Alkaline Phosphatase, Intestinal	**F**	ACAGCCACCAGGATCCTAAA
			R	CTTCCTATCGCAGGGGTTG				**R**	TTTGCTGATCACTTTGCACAT				**R**	GCACCTGTCTGTCCACATTG
8	**PIWIL4**	piwi-like RNA-mediated gene silencing 4	**F**	CCCGAGTGAAGGCCAGAG	22	**MAP2K6**	mitogen-activated protein kinase kinase 6	**F**	GACTCCAAGGCTTGCATTTCT	37	**ALPG**	Alkaline Phosphatase, Germ Cell	**F**	ACAGCTGCCAGGATCCTAAA
			R	GATCCTGCTTGTTCCCAAGA				**R**	CACGTGCCGCATCTTCTC				**R**	TGTCTGGCACATGCTTGTCT
9	**SALL4**	spalt-like transcription factor 4	**F**	ACCCCGGAGTTTGCAGAT	23	**TGFA**	transforming growth factor alpha	**F**	TGTTCGCTCTGGGTATTGTG	38	**ALPP**	Alkaline Phosphatase, Placental	**F**	
			R	GACGAAGCCGCTTTACTGTG				**R**	GGGAATCTGGGCAGTCATTA				**R**	
10	**MAPK4**	mitogen-activated protein kinase 4	**F**	CATCCTGGCTGAGATGCTTA	24	**STON2**	stonin 2	**F**	GACGACTTTGGACCATGTGA	39	**SOX2**	SRY-Box Transcription Factor 2	**F**	ACTTTTGTCGGAGACGGAGA
			R	AGCAGCTCGTCCTTGTCTTC				**R**	GACTGGTCTGGGGAAGATGA				**R**	CATGAGCGTCTTGGTTTTCC
11	**MDK**	midkine (neurite growth-promoting factor 2)	**F**	GAAGAAGGCGCGCTACAAT	25	**SYTL1**	synaptotagmin like 1	**F**	TGACAGAGGAGGAGCAGGAG	40	**NANOG**	Nanog Homeobox	**F**	AGATGCCTCACACGGAGACT
			R	GGCTTGGCGTCTAGTCCTTT				**R**	AACCAGTCCCCTGTCAGGAT				**R**	TTTGCGACACTCTTCTCTGC
12	**WISP2**	WNT1 inducible signaling pathway protein 2	**F**	ATGAGAGGCACACCGAAGAC	26	**GAP43**	growth associated protein 43	**F**	TGAGAAGAACCAAACAGGTTGA	41	**LIF**	Leukemia inhibitory factor	**F**	CTATGTGGCCCCAACGTGA
			R	GTACTCCCAGCGGGCATC				**R**	TGTTATGTGTCCACGGAAGC				**R**	TTGAGGATCTTCTGGTCCCG
13	**BMP7**	bone morphogenetic protein 7	**F**	GCCTGCAAGATAGCCATTTC	27	**SYTL5**	synaptotagmin like 5	**F**	CTGGGCGTCCTAAAGAGAGA	42	**IL6**	Interleukin 6	**F**	CCACTCACCTCTTCAGAACG
			R	TGGAAAGATCAAACCGGAAC				**R**	GCTGGCCTCTTGTTGAGTTT				**R**	AGGTTCAGGTTGTTTTCTGCC
14	**BARX1**	BARX homeobox 1	**F**	GGGCGAGCTGCTGAAGTT	28	**OCT4-1**	OCT4 Complete	**F**	CTTGGGCTCGAGAAGGATGT	43	**GAPDH**	Glyceraldehyde 3-phosphate dehydrogenase	**F**	GAAGGTGAAGGTCGGAGT
			R	AGAGCTCAGCCCTGAACAGC				**R**	CTGAGAAAGGAGACCCAGCA				**R**	GAAGATGGTGATGGGATTTC
15	**WNT9A**	wingless-type MMTV integration site family member 9A	**F**	CTCGAGTGCCAGTTCCAGTT	29	**OCT4A1-1**	OCT4A1 Isoform - First Round	**F**	GAGAAGGAGAAGCTGGAGCA					
			R	CGAGGAGATGGCATAGAGGA				**R**	CCTGTGTATATCCCAGGGTGA					

Table 1: PCR Primers for Gene Expression Analysis

Multivariate Parameter	B0/B1 Estimate	P-Value	Multivariate Parameter	B0/B1 Estimate	P-Value	Multivariate Parameter	B0/B1 Estimate	P-Value
OCT4A1 = sample*Xi + Ei	4.00	0.0004	OCT4B1 = sample*Xi + OCT4C*Xi + Ei	6.30	0.0193	OCT4A2 = sample*Xi + NANOG*SOX2*Xi + Ei	6.80	0.0235
OCT4A2 = sample*Xi + Ei	7.03	0.0004		-0.04	0.8861		0.01	0.9075
OCT4A3 = sample*Xi + Ei	6.30	0.0003	OCT4B2 = sample*Xi + OCT4C*Xi + Ei	1.32	0.7545	OCT4A3 = sample*Xi + NANOG*SOX2*Xi + Ei	5.24	0.0281
OCT4B1 = sample*Xi + Ei	6.03	<.0001		0.78	0.2242		0.03	0.5049
OCT4B2 = sample*Xi + Ei	6.75	0.0004	OCT4A1 = sample*Xi + OCT4B1*OCT4B2*Xi	4.24	0.017	OCT4B1 = sample*Xi + NANOG*SOX2*Xi + Ei	4.82	0.0002
OCT4C = sample*Xi + Ei	6.94	<.0001		-0.01	0.8243		0.03	0.0423
LIF = sample*Xi + Ei	6.45	0.0005	OCT4A2 = sample*Xi + OCT4B1*OCT4B2*Xi	6.54	0.0254	OCT4B2 = sample*Xi + NANOG*SOX2*Xi + Ei	3.23	0.0196
IL6 = sample*Xi + Ei	0.99	0.0452		0.02	0.798		0.09	0.0079
SOX2 = sample*Xi + Ei	5.37	<.0001	OCT4A3 = sample*Xi + OCT4B1*OCT4B2*Xi	5.09	0.0281	OCT4A1 = sample*Xi + LIF*IL6*Xi + Ei	1.63	0.5907
NANOG = sample*Xi + Ei	5.05	0.0099		0.04	0.4363		-0.17	0.4319
OCT4A1 = sample*Xi + OCT4C*Xi + Ei	2.15	0.4596	OCT4B1 = sample*Xi + OCT4A1*OCT4A2*OCT4A3*Xi	6.38	0.0002	OCT4A2 = sample*Xi + LIF*IL6*Xi + Ei	3.59	0.5047
	0.27	0.5115		-0.01	0.5279		-0.25	0.5132
OCT4A2 = sample*Xi + OCT4C*Xi + Ei	0.28	0.9437	OCT4B2 = sample*Xi + OCT4A1*OCT4A2*OCT4A3*Xi	6.36	0.0136	OCT4A3 = sample*Xi + LIF*IL6*Xi + Ei	1.69	0.6836
	0.97	0.1239		0.01	0.786		-0.33	0.2837
OCT4A3 = sample*Xi + OCT4C*Xi + Ei	1.50	0.6843	OCT4A1 = sample*Xi + NANOG*SOX2*Xi + Ei	4.11	0.0203	OCT4B1 = sample*Xi + LIF*IL6*Xi + Ei	6.55	0.0217
	0.69	0.2183		0.00	0.9229		0.04	0.8006
						OCT4B2 = sample*Xi + LIF*IL6*Xi + Ei	6.79	0.2395
							0.00	0.9938

Table 2: Linear and Multivariate Regression

Analysis of OCT4 isoforms, Stem Markers, and cell-cell signaling factors was completed with SAS computing software utilizing the 'procglm' function to determine the statistical relationship amongst various parameters comparing correlations amongst genetic expression using qt-PCR normalized cycle threshold values

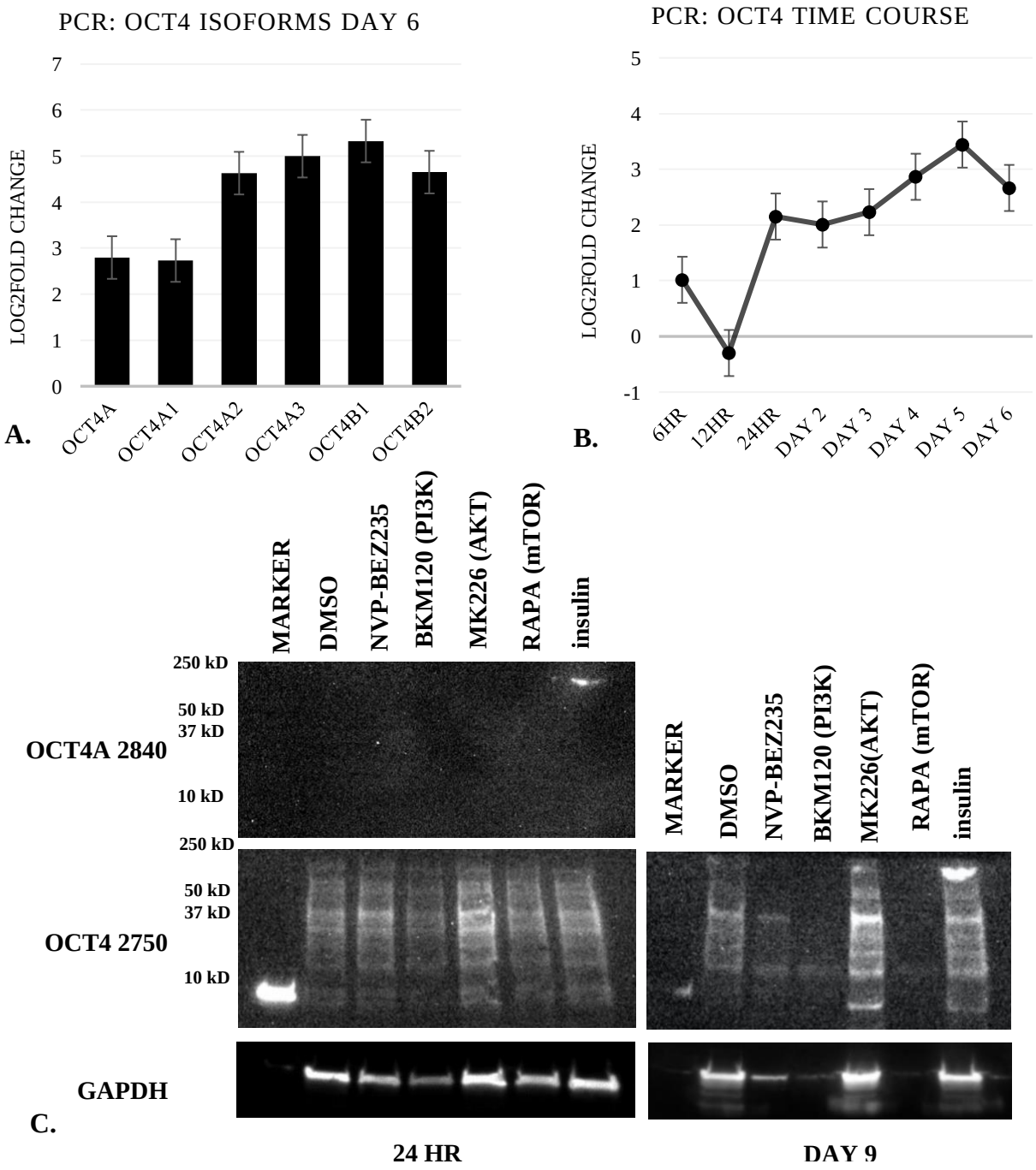

Figure 1: OCT4 Gene and Protein Expression

(A) PCR results of analyzing OCT4 isoform genetic expression at day 6 timepoint

(B) PCR results of analyzing ALP isoform genetic expression at day 6 timepoint

(C) 24 hr vs. 9 days Western Blot of OCT4 complete antibody and OCT4A region of protein; cells treated with various drugs that inhibit PI3K/mTOR/AKT pathways

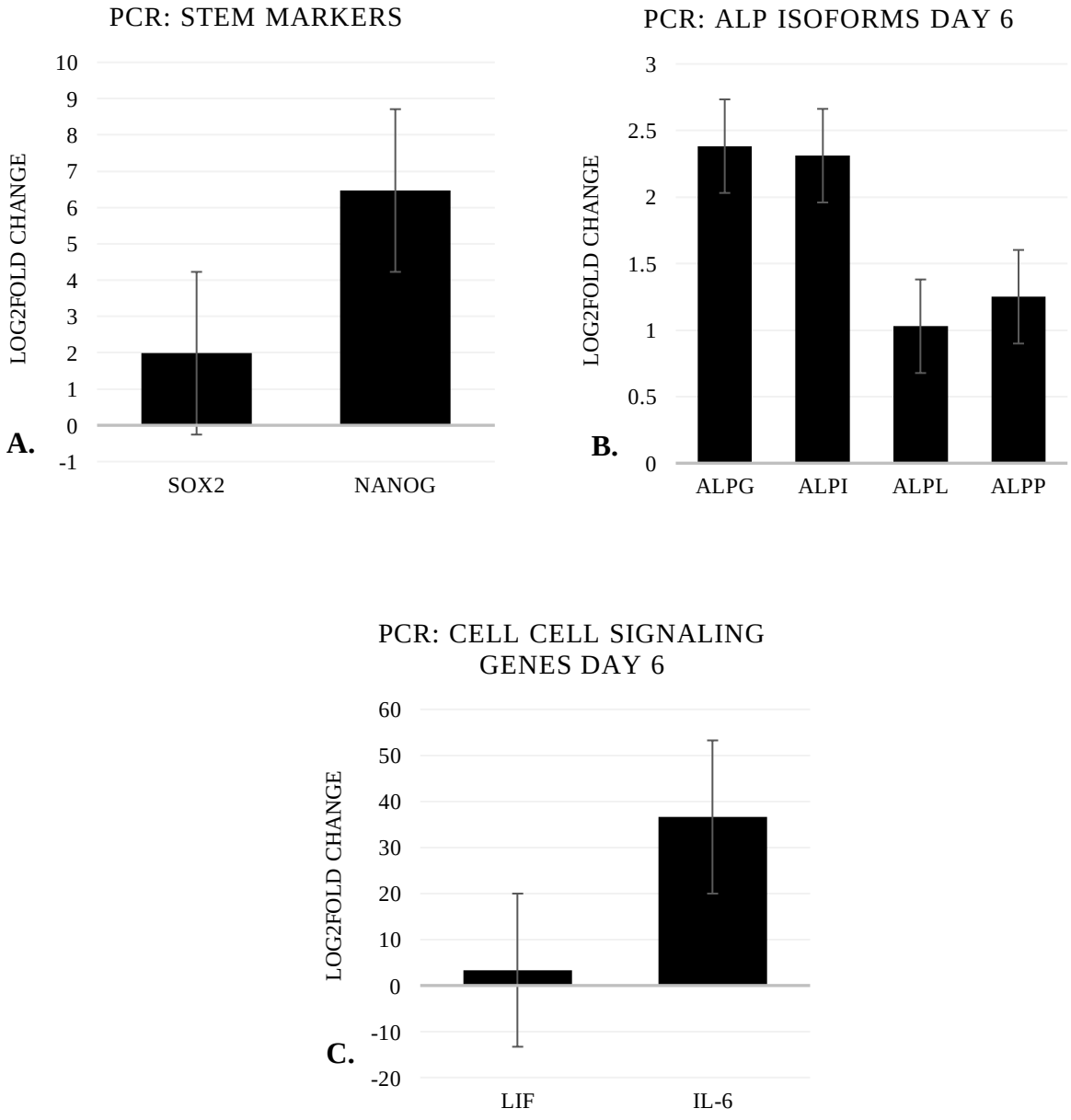

Figure 2: Stem Marker and Cell-Cell Signaling Gene Expression

(A-C) PCR results for analyzing the genetic expression of stem cell markers SOX2 and NANOG; cell-cell signal factors LIF and IL-6 both at a day 6 timepoint after being treated with NVP-BEZ235

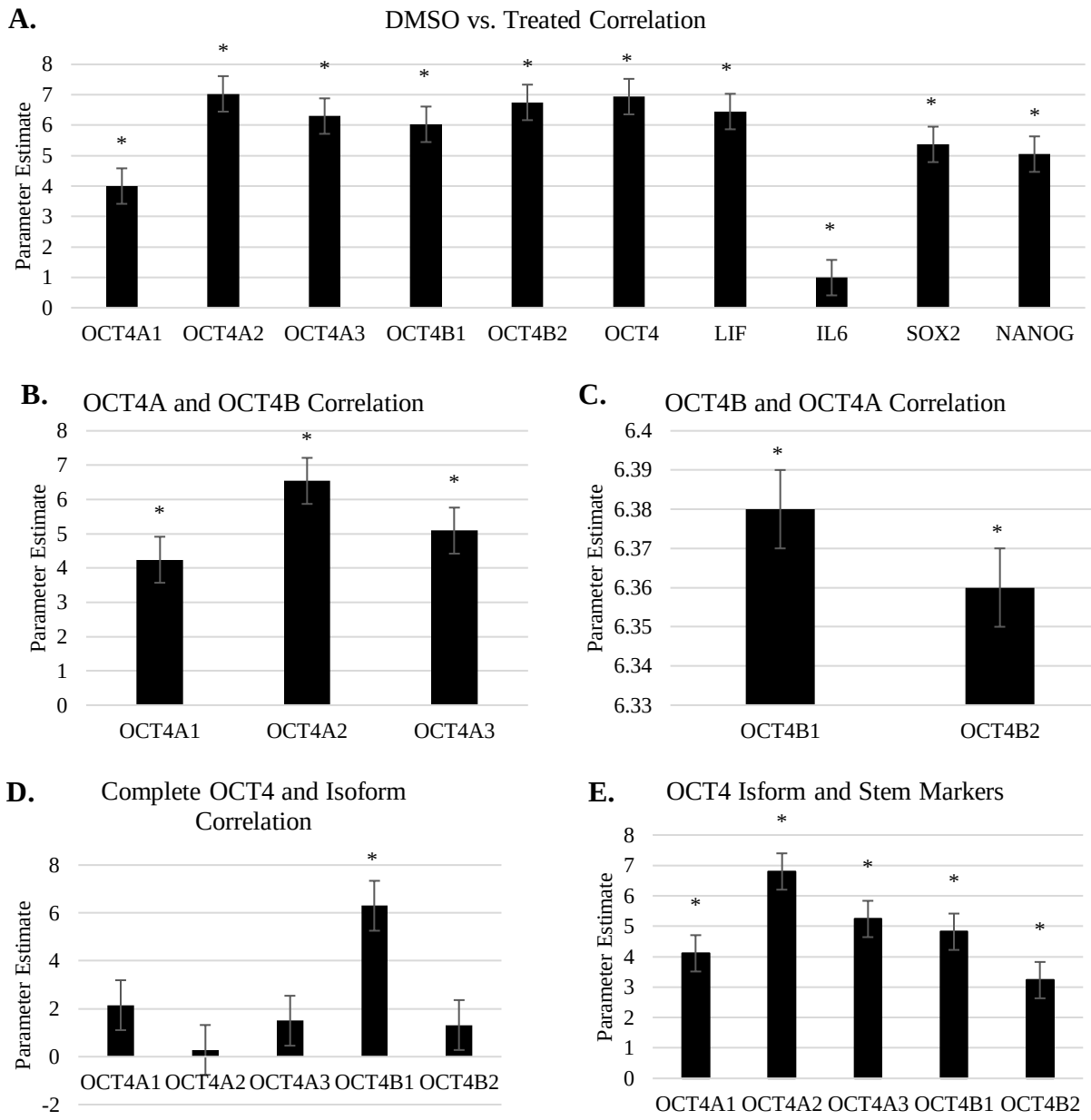

Figure 3: Regression Analysis

(A – F) Several genomic circumstances were analyzed statistically for significance utilizing linear and multivariate regression models; 'procglm' function was used in SAS software. Cycle threshold datapoints from qt-PCR were utilized as incremental variables representing expression levels. Parameter Equation, Statistical P-Value, Parameter Values are listed in Table 2

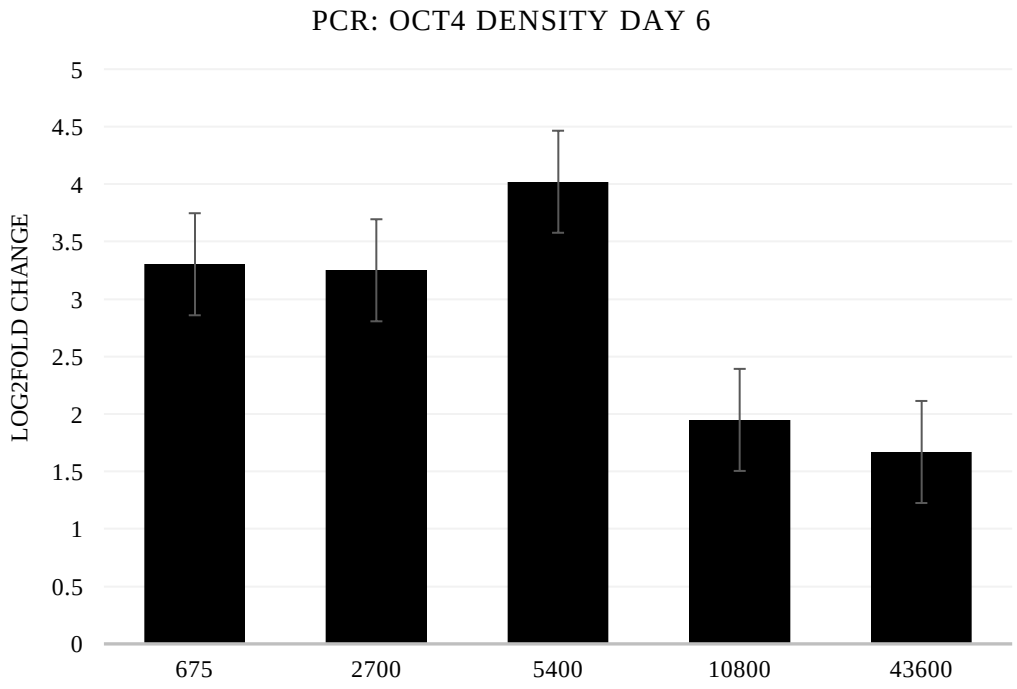

Figure 4: OCT4 Genetic Expression in Cell Density for RNA-Seq Optimization

Qt-PCR analysis was utilized to determine which day for the treated samples would allow for an adequate cellular population with a high enough RNA integrity.

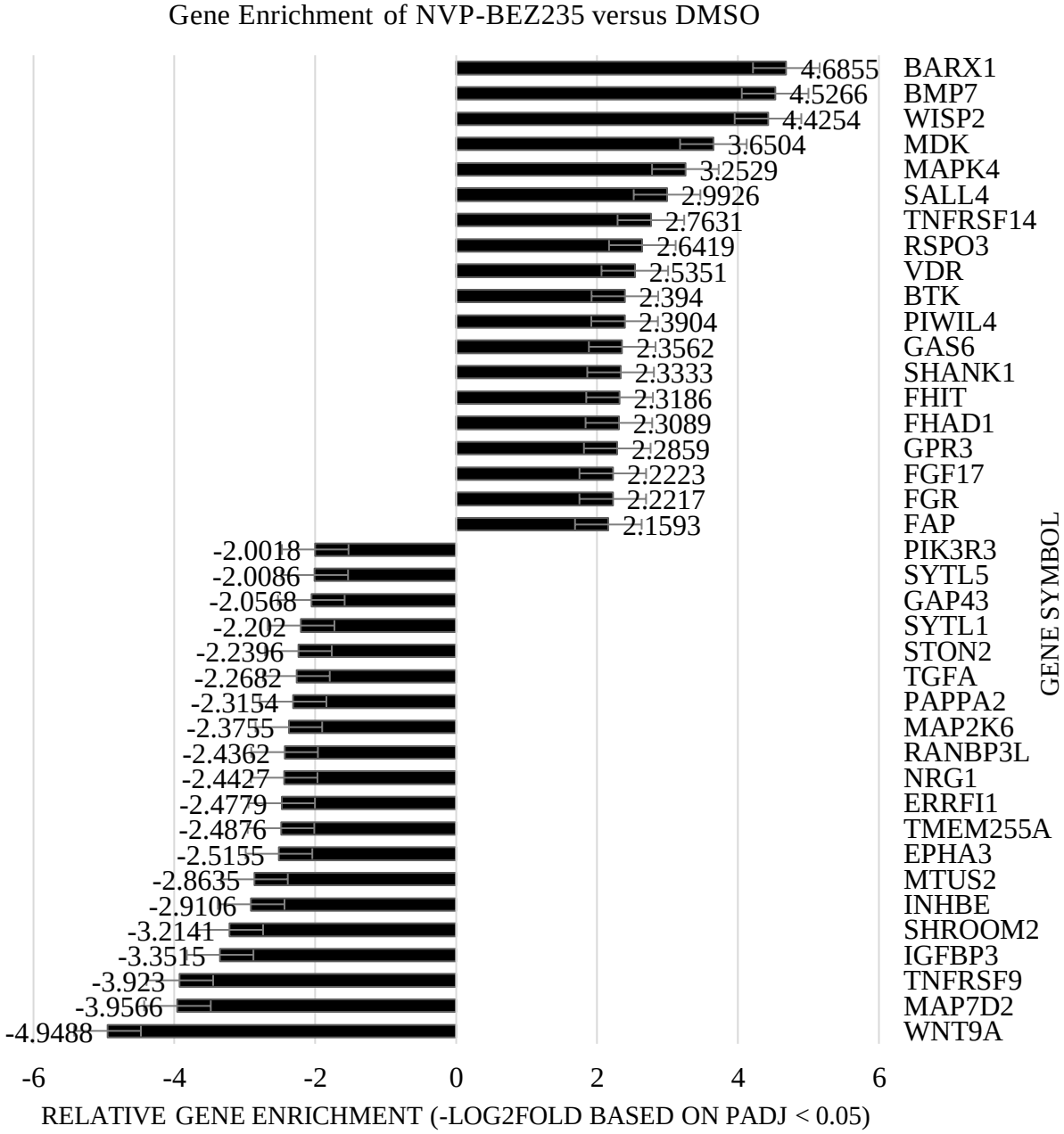

Figure 5: 40 Highest Differentially Expressed Genes from RNA-Sequence

The top 40 genes that were differentially expressed were categorized into being either upregulated (20) or downregulated (20) in the NVP-BEZ235 treated samples

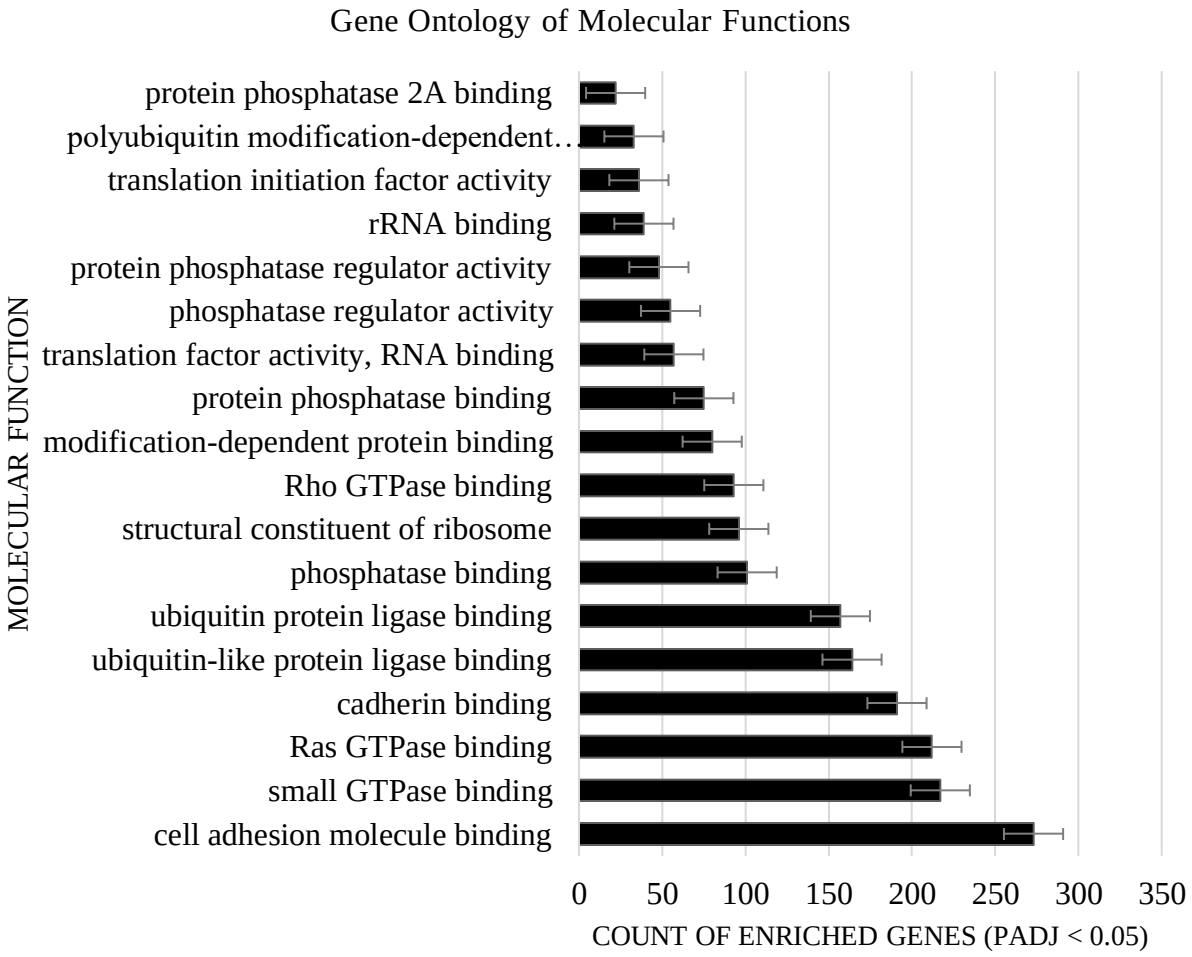

Figure 6: Differentiated GO of Molecular Functions

Various gene sets that focus on similar genes associated with a specific molecular function were analyzed using the normalized read datapoints from the differentially expressed genes in the RNA-seq

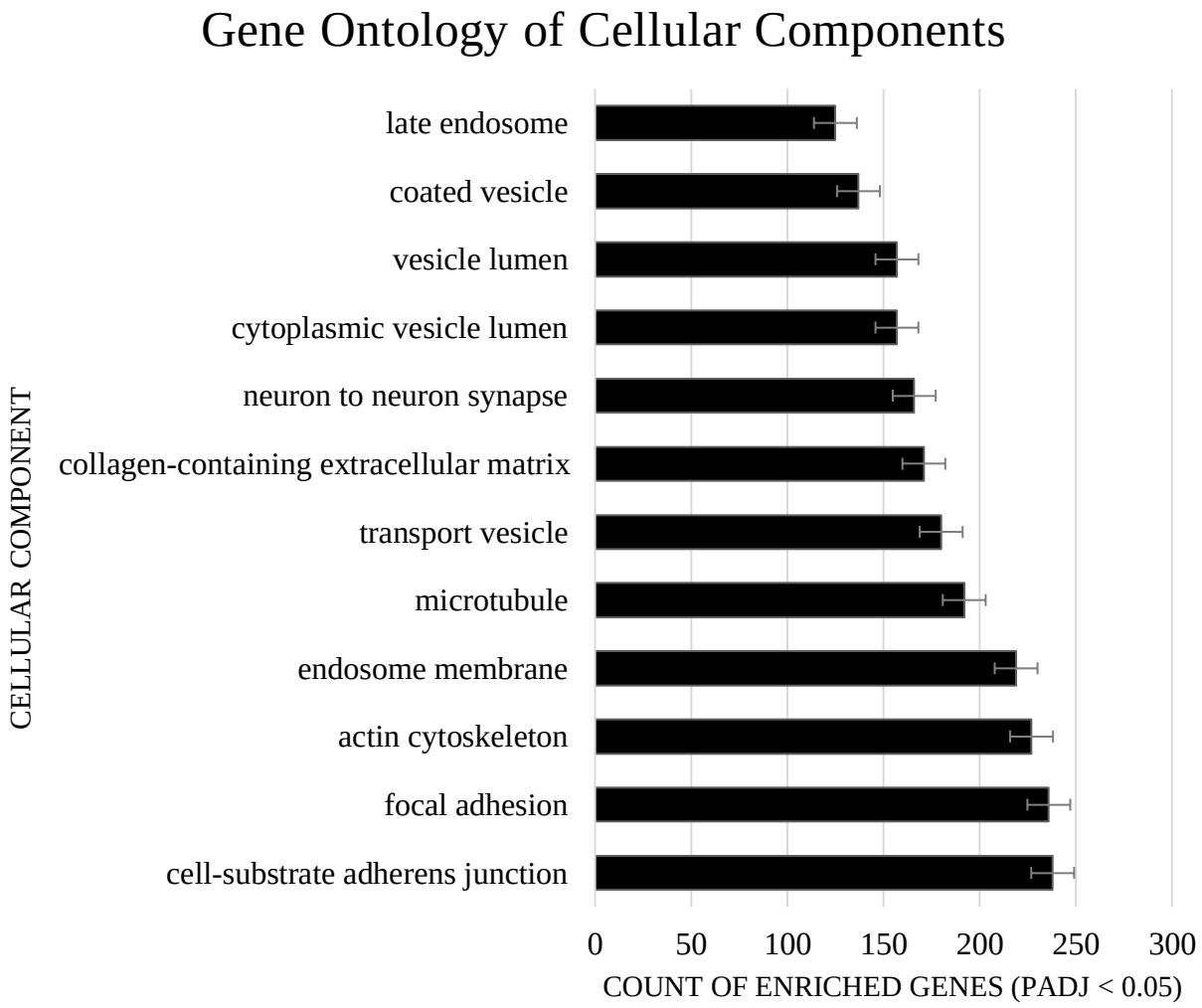

Figure 7: Differentiated GO of Cellular Components

Various gene sets that focus on similar genes associated with a specific cellular component were analyzed using the normalized read datapoints from the differentially expressed genes in the RNA-seq

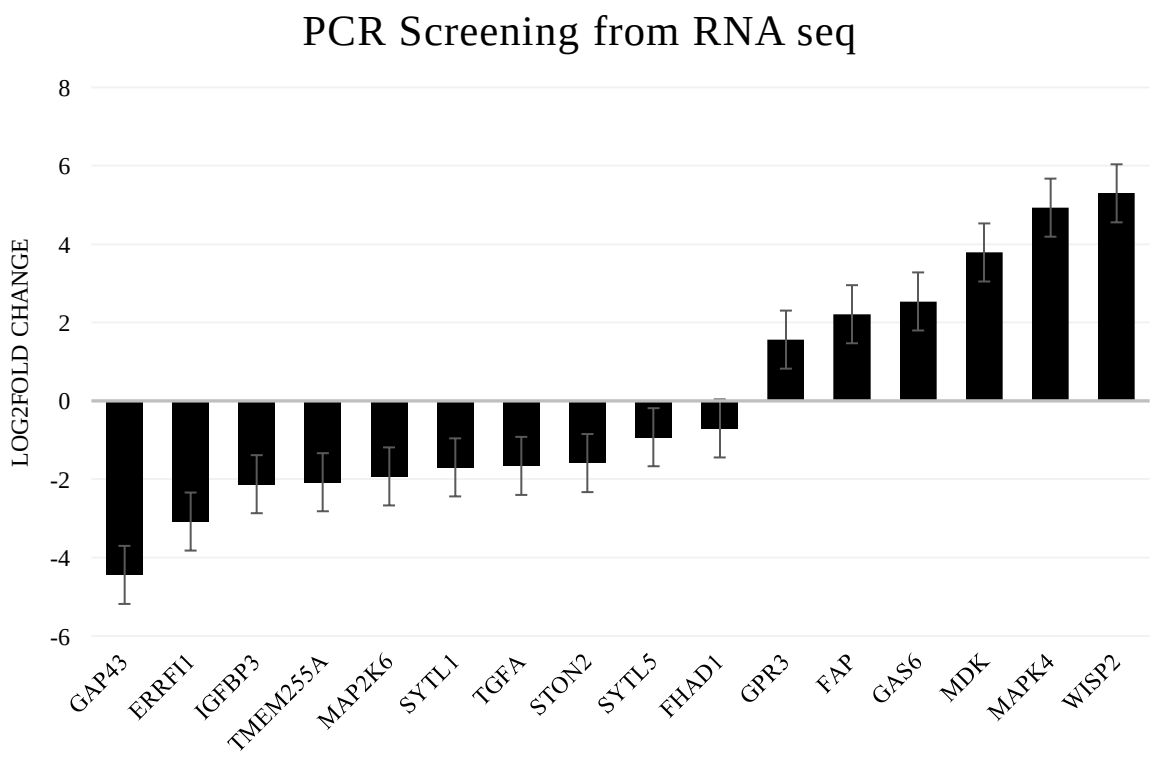

Figure 8: PCR Screening Confirmation for RNA-Sequencing Results

25 Primers designed and listed in table 1 were tested for utilizing qt-PCT to determine the confirmation of differentially expressed genes from the RNA-seq results.

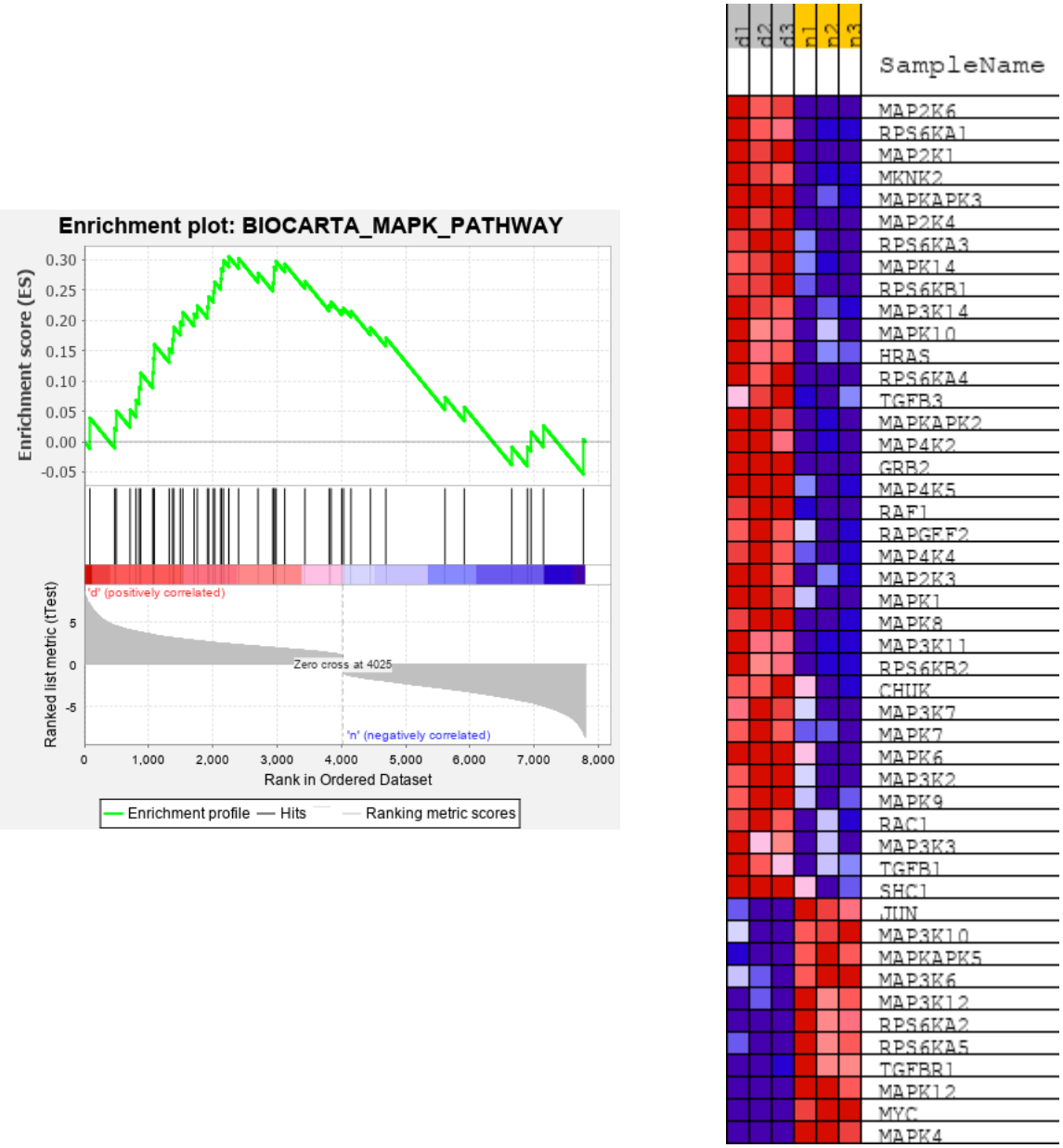

Figure 9: Gene Set Enrichment Analysis (GSEA) Analysis for mitogen activated protein kinase (MAPK) pathways

(A) Gene Set Enrichment Analysis (GSEA) Plot

(B) Heatmap of Differentially expressed MAPK Factors

BIOGRAPHICAL SKETCH

At the age of 15, Carl George Litif Jr. began his collegiate journey at the University of Texas Rio Grande Valley (UTRGV) undertaking the study of biological sciences. While completing his undergraduate degree at UTRGV, Mr. Litif participated in ecological and organic chemistry research for 18 months under Dr. Andrew McDonald and Dr. Jose Gutierrez-Gonzalez, respectively. Carl Litif was employed by UTRGV as a supplemental instructor during the latter of his undergraduate career for biology II courses. After successful graduation in December 2018 with a degree of Bachelor of Science in Biological Sciences at the University of Texas Rio Grande Valley, Mr. Litif went on to continue his studies in biology by pursuing a degree of Master of Science in Biology at the University of Texas Rio Grande Valley.

Researching under Dr. Megan Keniry, Mr. Litif completed novel work on the genetic alterations involved in specific glioblastoma types. While partaking in research, Mr. Litif assisted in teaching the lab portions of lower level anatomy and physiology and upper level cell biology courses. Mr. Litif defended his thesis on glioblastoma and earned his degree of Master of Science in Biology at the University of Texas Rio Grande Valley in August 2020. Carl's growing passion for building his molecular and genetic biological knowledge led him to achieve acceptance into the fall 2020 entering class of the Molecular and Life Science doctoral program at the University of Wyoming. After five years of PhD candidacy, Carl plans on pursuing his post-doctoral career, and eventually he sees himself coercing the foundation of a research institution intended to expand the biological community into regions that are less exposed or financially incapable. You can reach Carl Litif at clitif@uwyo.edu or by mail at 1856 W Harrison St. Apt C1, Laramie, Wyoming 82070.